

Measurements of photoelectron angular distributions by single-photon detachment of Al^- , Si^- , and P^- at visible photon wavelengths

A. M. Covington, D. Calabrese, W. W. Williams, and J. S. Thompson

Department of Physics and Chemical Physics Program, University of Nevada, Reno, Nevada 89557-0058

T. J. Kvale

Department of Physics and Astronomy, University of Toledo, Toledo, Ohio 43606-3390

(Received 30 May 1997)

The spectral dependence of the angular distributions of photoelectrons produced by the single-photon detachment of Al^- , Si^- , and P^- ions has been measured at five discrete photon wavelengths ranging from 457.9 to 647.1 nm (2.71–1.92 eV) using a crossed laser-ion beam apparatus. Values of the asymmetry parameter have been determined by fits to the photoelectron yield as a function of the angle between the laser polarization vector and the linear momentum vector of the collected photoelectrons. The experimental results for Al^- are compared with a recent theoretical calculation [C. N. Liu and A. F. Starace, *Bull. Am. Phys. Soc.* **42**, 1026 (1997)] and are found to be in good agreement.

[S1050-2947(97)07412-X]

PACS number(s): 32.80.Gc, 32.10.-f, 33.60.-q

I. INTRODUCTION

The phenomenon of photodetachment, where a negative ion absorbs a photon of sufficient energy to revert to a neutral atom plus a free electron, has been the subject of intensive theoretical and experimental study in recent years. Photodetachment processes have been determined to be the main source of opacity in the solar photosphere at red and infrared wavelengths [2,3]. Furthermore, both photodetachment and its inverse process, radiative electron attachment, play essential roles in regulating the density of free electrons in the *D* region of the Earth's ionosphere, and contribute to atmospheric conductivity [4]. Negative ions are also important in both gas-phase chemistry and low-temperature plasmas. Negative-ion research has proven germane in the development of a variety of applied technologies such as negative-ion sources, Penning discharge devices, air purifiers, photodetachment microscopes, and neutral beam injectors [5].

Fundamental experimental and theoretical studies of the photodetachment of negative ions provide information necessary to characterize the initial and final states of the target species, as well as dynamical information pertaining to the mutual interaction of collision partners [6]. Photodetachment studies provide a unique opportunity to examine electrons liberated from a neutral core. Therefore, subtle interactions such as electron correlation and relativistic effects, which might be overshadowed by the long-range Coulomb potential present in the photoionization of either neutral or positively charged ionic species, can be studied in photodetachment processes.

A. Previous theoretical work

As opposed to calculations of total photodetachment cross sections, differential cross-section calculations explicitly depend on both the magnitude and relative phases of transition

amplitudes. Hence, differential cross-section calculations can be used to obtain both the yield and angular distributions of photoelectrons. The most general form of the angular distribution of a collision process for an unpolarized target can be summarized by the following theorem derived by Yang [7]: "If only incoming waves of orbital angular momentum L contribute appreciably to the reaction, the angular distribution of the outgoing particles in the center of mass system is an even polynomial of $\cos\theta$ with maximum exponent not higher than $2L$." Here θ is the angle between the incoming and outgoing particles in the center-of-mass system. It should be noted that the angular distribution does not contain a term linear in $\cos\theta$ since parity is conserved in a photoabsorption process. In the later, negative-ion specific development of Cooper and Zare [8,9], the differential cross section for the production of photoelectrons detached from a randomly polarized target (i.e., statistical population of all degenerate states) by incident linearly polarized light, can be written in the dipole approximation as

$$\frac{d\sigma}{d\Omega} = \frac{\sigma}{4\pi} \left[1 + \frac{\beta}{2} (3 \cos^2\theta - 1) \right], \quad (1)$$

where σ is the total photodetachment cross section at a given photon energy and β is the asymmetry parameter, which completely characterizes the shape of the photoelectron emission pattern. Since the differential cross section must have a non-negative value, the asymmetry parameter is restricted to the range $-1 \leq \beta \leq 2$. Within the independent-particle approximation, the asymmetry parameter β for the photoejection of an electron from an initial state with angular momentum l is given by [8],

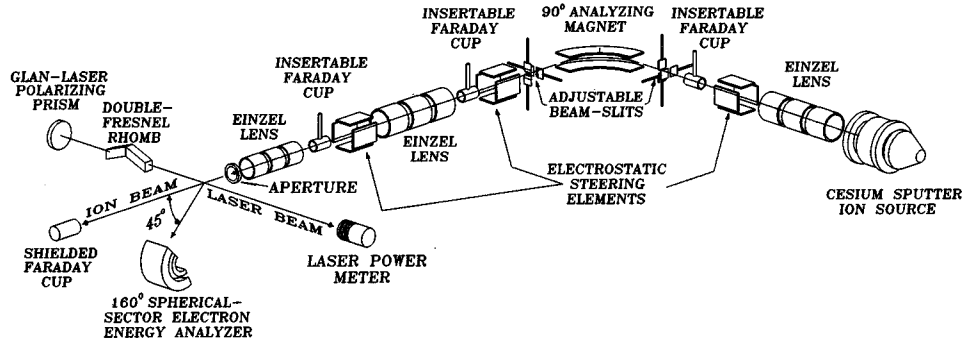


FIG. 1. Schematic diagram of the experimental apparatus. See text for details.

$$\beta = \frac{l(l-1)\sigma_{l-1}^2 + (l+1)(l+2)\sigma_{l+1}^2 - 6l(l+1)\sigma_{l+1}\sigma_{l-1}\cos(\delta_{l+1} - \delta_{l-1})}{(2l+1)[l\sigma_{l-1}^2 + (l+1)\sigma_{l+1}^2]} \quad (2)$$

The asymmetry parameter is found to be most sensitive to the phase-shift differences $\delta_{l+1} - \delta_{l-1}$, though it is also dependent upon the relative magnitudes of the radial dipole integrals σ_{l+1} and σ_{l-1} .

Spectral variations of photoelectron angular distributions in the vicinity of resonances [10] have been predicted to depart markedly from those predicted for direct (nonresonant) photoprocesses such as the model of Cooper and Zare. The energy dependence of the asymmetry parameter in this case is due to configuration interaction, which allows for alternative final-state channels for the liberated photoelectron. Spectral variation of the asymmetry parameter may also be enhanced near cross-section minima, due to rapid changes in the relative magnitudes of the amplitudes for the various channels [11]. A more detailed theoretical description of the photodetachment process must also consider the final-state interaction between the photoelectron and its parent residual atom. The coupling of the outgoing electron partial waves to the residual atom can result in various photodetachment channels. Using the angular-momentum transfer theory formalism of Fano and Dill [12], this coupling produces allowed angular-momentum transfers from the photon to the ion expressed by $\mathbf{j}_i = \mathbf{L}_c - \mathbf{L}_0$. Here \mathbf{L}_c and \mathbf{L}_0 are the orbital angular momenta of the residual atomic core and negative ion, respectively. Within the electric dipole and LS coupling approximations, parity conservation assigns values that are either parity favored [$\pi_0\pi_c = (-1)^{j_i}$] or unfavored [$\pi_0\pi_c = (-1)^{j_i+1}$]. Within this formalism, the effective value of the asymmetry parameter β can be written as a weighted average of the form

$$\beta = \frac{\sum_{j_i} \sigma(j_i)\beta(j_i)}{\sum_{j_i} \sigma(j_i)}, \quad (3)$$

where the summation extends over all allowed values of j_i , and $\beta(j_i)$ and $\sigma(j_i)$ are the asymmetry parameters and partial photodetachment cross sections characteristic of a given value of j_i . Both the photodetachment cross sections and

asymmetry parameters can be expressed in terms of photodetachment scattering amplitudes $S_l(j_i)$ where l is the orbital angular momentum of the photoelectron and is restricted to the value $j_i \pm 1$ or j_i .

B. Previous experimental work

Photodetachment experiments were pioneered in 1954 by Branscomb and Smith [13,14]. These experiments employed the then novel crossed-beam technique, in which a H^- -ion beam was crossed perpendicularly with a photon beam produced by a tungsten lamp. The advent of lasers along with high-resolution electron spectrometers ushered in a myriad of experimental studies utilizing similar techniques. The first detailed experimental study of angular distributions of photodetached electrons was conducted by Hall and Siegel in 1968 [15]. Photoelectron angular distributions were measured for H^- , C^- , and O^- at 488.0- and 514.5-nm photon wavelengths. Subsequent studies have been carried out on several different species [16], but with few exceptions [17–19], most have not involved a wide range of photon wavelengths. Traditionally, these experiments have been difficult, owing to the limited number of available laser wavelengths of sufficient photon intensity and the difficulty of production of adequate beam currents needed to realize acceptable signal-to-noise ratios. This paper presents a systematic experimental study of photoelectron angular distributions of Al^- , Si^- , and P^- at visible photon wavelengths. These measurements are part of an ongoing study of the fundamental physical interactions underlying the photodetachment phenomena.

II. EXPERIMENT

A schematic diagram of the experimental apparatus is shown in Fig. 1. The negative-ion beams are produced with a commercial cesium-sputter negative-ion source [20]. Details of source operation are given elsewhere [21,22]; however, a brief description of the operation of the negative ion source used for this set of experiments is given here. Positively charged cesium ions are accelerated to energies ranging from

~ 2 to 6 keV toward a negatively biased, cesium-coated pellet containing the element under study. The sputtering acceleration voltage was adjusted until optimal negative ion-beam currents were extracted. Typical operational vacuum in the source was 2.7×10^{-5} Pa. Sputtering from the pellets produces low-velocity negatively charged atoms and molecules that are accelerated away from the pellet through an exit aperture, and are further accelerated as they approach the extraction electrode. The sputter probe was maintained between -5 to -30 kV with respect to ground. After leaving the extraction region, the negative-ion beams were focused and then momentum analyzed using a postacceleration 90° bending magnet with a mass resolution of ~ 200 . Two-dimensional, adjustable beam slits were installed at the entrance and exit foci of the magnet in order to reduce aberration in the ion beam. Typically, the beam slits were set to an area of 36 mm^2 . The ion beam was then focused with a pair of Einzel lenses and collimated with apertures before entering the experimental chamber. The postmagnet section of the beam line was differentially pumped and was typically maintained at 4×10^{-7} Pa in order to minimize degradation of the negative-ion beam through collisional detachment processes. After entering the chamber, the ion beam was crossed by a laser-produced linearly polarized photon beam at an intersection angle of 90° . The ions had traveled a total distance of ~ 6.4 m upon reaching the intersection with the laser beam. The typical pressure in the interaction region was maintained at $\sim 1 \times 10^{-6}$ Pa.

The photon beams (457.9, 476.5, 488.0, and 514.5 nm) were produced by either a 25 W Coherent Sabre R or a 5 W Spectra Physics 2045 argon-ion laser operating in single line mode. Red light (647.1 nm) was generated with a 1 W Spectra Physics Model 2030 krypton-ion laser operating in multiline mode. An external prism was used for wavelength selection for the krypton-ion laser. The linear polarization of the photon beam was ensured by a Glan-Laser polarization prism with an extinction ratio of 5×10^{-5} . Rotation of the linear polarization about the laser axis was accomplished through the use of a $\lambda/2$ phase retarder (double Fresnel rhomb) mounted in a micrometer-driven rotational stage. The output power level of the laser was monitored with a power meter, and the ion-beam current was collected in a shielded Faraday cup. Both signals were continuously monitored and recorded for normalization of the photoelectron data.

Electrons photodetached in the interaction region were energy analyzed using a spherical-sector, 160° electrostatic kinetic-energy analyzer operated in fixed pass-energy mode. Typical pass energies of 20–40 eV were used for all measurements. The mean radius of the spectrometer is 3.81 cm. A set of 0.5-mm-diam entrance apertures leading into the spectrometer are spaced 5 mm apart. The first entrance aperture is 3.18 cm from the center of the interaction region. This geometry limits the acceptance angle of the spectrometer to less than 1° . The electron spectrometer is situated with its symmetry axis in the plane that is perpendicular to the plane formed by the ion and laser beam axes, and contains the ion-beam velocity vector. The spectrometer is mounted in a goniometric cradle, and can be rotated from a 45° to 90° declination angle with respect to the ion-beam axis in order to facilitate systematic studies of kinematic effects. For all

the measurements presented in this paper, the spectrometer was located at a 45° declination angle.

In the geometry of this experiment, a kinematic adjustment to the measured photoelectron energies must be made in order to correct for differences between electrons detached from the center-of-mass (ion) frame and measured in the laboratory (rest) frame of reference. A transformation equation relating photoelectron kinetic energy in the ion frame E_C with its corresponding energy in the laboratory frame E_I is given by [23]

$$E_C = E_I + \varepsilon - 2\sqrt{\varepsilon E_I} \cos \theta_I, \quad (4)$$

where $\varepsilon = (1/2)m_e v_i^2$ is the kinetic energy of an electron moving with the same velocity v_i as an ion in the beam, and θ_I is the angle subtended between the electron's laboratory velocity vector and the velocity vector of an ion in the beam. Solving Eq. (4) for the laboratory energy yields two physical solutions corresponding to photoelectrons ejected in the forward (spectrometer) and backward directions. As a result of these kinematic effects, only photoelectrons ejected with momentum vectors in the forward direction were detected in the 45° declination angle geometry.

The relatively low laboratory-frame electron energies (< 3 eV) necessitated that care be taken to reduce the effects of stray electric and magnetic fields in the experimental chamber. In order to minimize possible contact potentials, all materials in the vicinity of the electron spectrometer were coated with Aerodag G. The Earth's and residual magnetic fields were nulled in the interaction region by Helmholtz coils surrounding the entire experimental chamber. In addition, a 1.5-mm thickness mu-metal shielding box was placed around the interaction region and electron spectrometer. Within the magnetic shielding, only nonmagnetic materials were used for construction of the apparatus. Measurements of the fields inside the shielding with a Hall probe gaussmeter indicated that stray magnetic fields had a magnitude of less than 5 mG.

Electrons with the correct energy for transmission through the spherical-sector analyzer were detected with a channel electron multiplier (CEM) operated with a typical gain of $\sim 10^8$. Extreme care was taken to ensure that all high-voltage contacts on the CEM were electrostatically shielded from the interaction region. Subsequent electron pulses were amplified in succession by a preamplifier and amplifier. After amplification, electron pulses entered a constant fraction discriminator (CFD) set to a discrimination level of 0.38 V to discriminate against electronic noise not associated with the experiment. Signal pulses passing through the CFD were converted to +5 transistor-transistor logic (TTL) pulses and counted with a National Instruments model AT-MIO-16X multifunction input-output (I/O) board in a PC-based data acquisition and control system. Analog outputs from the ion-beam current and the laser power meters were converted to frequencies by a voltage-to-frequency converter, and logged with counters on the I/O board for normalization of electron counts.

Before each photoelectron kinetic-energy spectrum was measured, the overlap between the photon and ion beams was maximized. This was accomplished through the following procedure: (i) maximization of signal at the peak of the photoelectron spectrum was obtained by rastering the laser

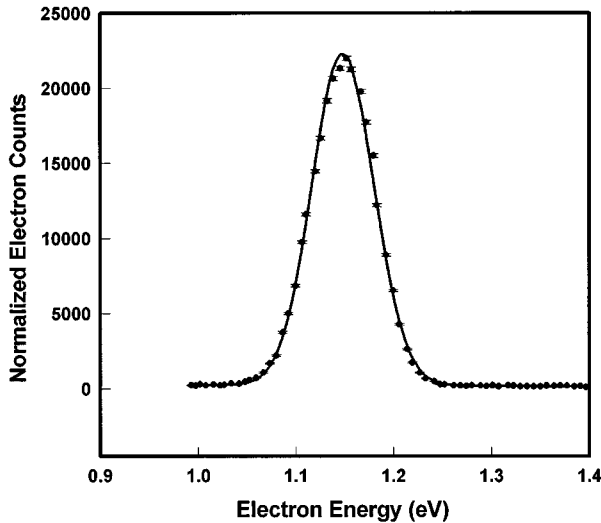


FIG. 2. Typical photoelectron energy spectrum for the photodetachment process $h\nu + C^-([\text{He}]2s^22p^3\ ^4S) \rightarrow C([\text{He}]2s^22p^2\ ^3P) + e^-(ks,d)$ at a photon wavelength $\lambda = 514.5$ nm. The abscissa corresponds to the normalized number of electron counts, and the ordinate to the photoelectron's center-of-mass kinetic energy. The experimental data points (solid circles) are shown along with their statistical uncertainty to one standard deviation. Also shown are the results of a weighted nonlinear least-squares fit of a Gaussian curve with a linear background to the experimental data (solid line).

beam through the ion beam; (ii) once maximum signal yield was obtained, the laser polarization vector was rotated through 180° , where the signal yield should reproduce, and the same procedure was carried out again. Through iteration, the maximum signal yield was obtained at both ends of the scan spectrum while monitoring the laser power through the interaction region to ensure that the laser was normally incident to the surfaces of the double-Fresnel rhomb. A starting position was established by determining the polarizer angle for maximum photoelectron yield. Thereafter, measurements were made every 10° over a total range of 240° . The photoelectron and normalization signals were carefully monitored to avoid saturating the photodetachment process during the experiments.

III. MEASUREMENTS AND RESULTS

A. Experimental technique

The experimental technique for measuring photoelectron angular distributions for negative ions will be described in general in the following section. For these measurements, the negative-ion beams were produced with a solid sputter probe. Typical ion-beam energies were ~ 10 keV and ion-beam currents ranged from 20 nA to $1.0\ \mu\text{A}$, depending upon the material being sputtered. Ion- and laser-beam stabilities during these measurements were better than 98%. Signal-to-noise ratios were typically 100:1 near the peaks of the angular distribution scans. The electron spectrometer pass energy for these measurements was 20 eV, and each scan was made over a 1.0 eV laboratory energy range. This energy range was usually divided into 100 equal steps, each having an integration time of 2 sec. Fine-structure transitions for the negative ions presented in this report were indistin-

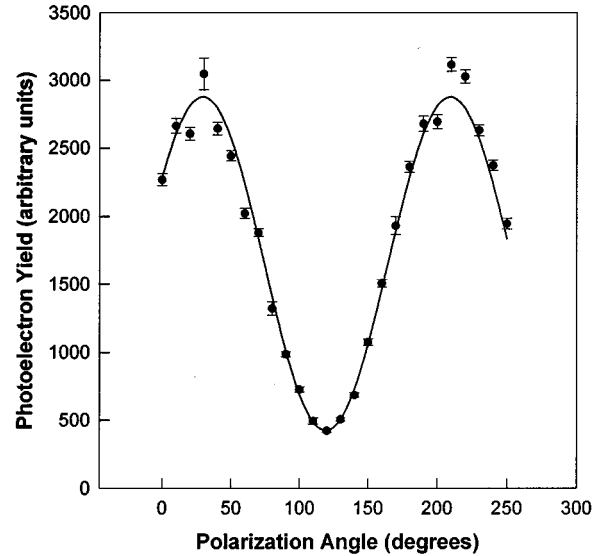


FIG. 3. Typical photoelectron yield-vs-linear polarization angle with respect to the linear momentum vector of the collected photoelectrons plot for benchmark measurements of C^- at a photon wavelength $\lambda = 514.5$ nm. The photoelectron yields (solid circles) are given along with error bars that reflect uncertainties in Gaussian fits used to determine the yields to one standard deviation. The solid line corresponds to a weighted nonlinear least-squares fit to the experimental data of the form $I(\theta) = a\{1 + \beta P_2[\cos(\alpha - c)]\}$. For this particular spectrum, the fit produced an asymmetry parameter of $\beta = -0.796 \pm 0.010$, which constrained the sign of the asymmetry parameter for all subsequent measurements.

guishable with the energy resolution of the electron spectrometer (~ 80 meV full width at half maximum) [16,24].

Following collection, each of the photoelectron spectra was fitted to the superposition of a Gaussian with a linear background that used a nonlinear least-squares-fitting routine that weighted each individual data point by its statistical uncertainty, assuming a Poisson distribution. Once the fitting parameters were obtained, each Gaussian was integrated in order to determine the total photoelectron yield along with its uncertainty at each indicated angle of the double-Fresnel rhomb α , which corresponds to the angle between the laser polarization vector and the electron collection direction. After determining the yields and uncertainties of each of the individual spectra, the asymmetry parameter was determined by a least-squares fit of photoelectron yield-vs-linear polarization angle with respect to electron collection direction data to the general expression $I(\theta) = a\{1 + \beta P_2[\cos(\alpha - c)]\}$, where $P_2(\cos\theta)$ is the second-order Legendre polynomial, and a , β , and c are fitting parameters.

The experimental technique was benchmarked with C^- [25] and compared to the previous measurements of Hall and Siegel [15] and the calculations of Cooper and Zare [8]. Figure 2 shows a typical electron energy spectrum of C^- along with a Gaussian fit of these data. A typical plot of photoelectron yield-vs-linear polarization angle with respect to the electron collection direction along with its fit is shown in Fig. 3. In this figure, the abscissa corresponds to the indicated dial reading α , not the angle θ . Hence, the appropriate sign of β is left undetermined. In order to determine the correct sign, a polarization analyzer with its axis parallel to

TABLE I. Asymmetry parameters for the photodetachment process $h\nu + C^-([\text{He}]2s^22p^3\ ^4S) \rightarrow C([\text{He}]2s^22p^2\ ^3P) + e^-(ks,d)$ at 1.145- and 1.277-eV photoelectron energies. The results of the current experimental measurements of the asymmetry parameter (β_{expt}) are tabulated along with experimental uncertainties to one standard deviation of the mean. Also shown are the previous experimental results (β_{prev}) of Hall and Siegel [15] as well as the theoretical results (β_{calc}) of Cooper and Zare [9].

Photon wavelength λ (nm)	Photoelectron energy (eV)	Asymmetry parameter β_{expt}	Asymmetry parameter β_{prev}	Asymmetry parameter β_{calc}
488.0	1.277	-0.72 ± 0.04	-0.715 ± 0.025	-0.65
514.5	1.145	-0.792 ± 0.012	-0.805 ± 0.025	-0.73

the electron collection direction was inserted into the laser beam after the double-Fresnel rhomb. Since β is approximately -1 for C^- at the photon energies measured, the indicated dial reading corresponding to $\theta=90^\circ$ (minimum electron yield) was calibrated, thereby determining the sign of β for all asymmetry parameters presented in this paper. At 488.0- and 514.5-nm laser wavelengths, repeated measurements were made on C^- and the results are tabulated in Table I. Also included in this table are the results of the previous measurements conducted by Hall and Siegel and the calculations of Cooper and Zare. The current experimental results are shown to be in excellent agreement with the previous experimental measurements, and in good agreement with the theoretical calculations. Experimental uncertainties for all angular distribution measurements include statistical and estimated systematic errors summed in quadrature as discussed below.

A Poisson distribution was assumed for counting statistics of each individual data points on each photoelectron kinetic-energy spectrum. Consequently, the counting statistics of each photoelectron spectrum were reflected in the uncertainties in the Gaussian fitting parameters. Uncertainties in the Gaussian fitting parameters, in turn, provided upper and lower bounds in the subsequent integrations to determine the photoelectron yield at each polarization angle. Following integration, uncertainties in the photoelectron yields were reflected in uncertainties of the fits for the determination of the asymmetry parameter, and are included to within one standard deviation. Typically, the weighted mean of all fits at each wavelength deviated by less than 5%. At each laser wavelength, a minimum of three and maximum of five individual scans were needed to realize this convergence. Systematic errors for all measurements are estimated to be less than 10%. These include contributions from time-dependent changes in the overlap of the ion and laser beams during the course of each scan as well as practically achievable alignment constraints. Uncertainties in both the reproducibility of the laser polarization angle and depolarization of the laser beam were determined to be negligible in comparison to the previously mentioned alignment errors.

B. Angular distributions of Al^-

The spectral dependence of the asymmetry parameter of Al^- was investigated by making angular distribution measurements at five discrete visible photon wavelengths (647.1, 514.5, 488.0, 476.5, and 457.9 nm). Al^- -ion beams were produced using either 6061 T-6 Al alloy or 99.999% pure Al as the sputter probe material. Ion-beam energies for measure-

ments were typically 10 keV. Al^- -ion beam currents ranged from 25 to 35 nA during all data scans, and laser power levels ranged from 0.35 W for the 647.1 nm to 7.5 W for the 514.5-nm wavelengths. These parameters yielded signal-to-noise ratios of 40:1 near the peaks of the photoelectron angular distributions.

Photodetachment from Al^- can be described by the following single-photon, single-electron process: $h\nu + Al^-([\text{Ne}]3s^23p^2\ ^3P) \rightarrow Al([\text{Ne}]3s^23p\ ^2P) + e^-(ks,d)$. Aluminum has a measured electron affinity of 0.44094 ± 0.00066 eV, which is the difference in the total binding energy of the $^2P_{1/2}$ neutral atom and the 3P_0 negative-ion ground states [26], thereby producing center-of-mass photoelectron energies ranging from 1.475 to 2.267 eV in these experiments. Contamination of the ion beam by the 1D_2 metastable negative-ion state was visible only once during the course of the experiment due to extreme overheating of the aluminum sputter probe. The metastable photodetachment peak was clearly resolved from the ground-state negative-ion photodetachment peak, demonstrating its absence during all other measurements. Figure 4 shows the results of a typical photoelectron yield-vs-polarization angle plot for Al^- at $\lambda=514.5$ nm. A summary of all measured asymmetry parameters for Al^- is given in Table II.

C. Angular distributions of Si^-

Angular distributions of photoelectrons were measured at photon energies ranging from 1.92 to 2.71 eV. Si^- beams were produced using a crystalline-Si sputter probe. Beam energies and currents were typically 10 keV and 1.5 μA , respectively. Signal-to-noise ratios near the peaks of the photoelectron angular distributions reached 300:1. Isotopic labeling of the ^{28}Si , ^{29}Si , and ^{30}Si stable isotopes produced relative abundances of 92:5:3, in good agreement with accepted values.

The single-photon detachment of Si^- can be described by the following process: $h\nu + Si^-([\text{Ne}]3s^23p^3\ ^4S) \rightarrow Si([\text{Ne}]3s^23p^2\ ^3P) + e^-(ks,d)$. The Si atom has an electron affinity of 1.385 eV and is defined as the difference in total binding energies between the 3P_0 ground state of the neutral atom and the $^4S_{3/2}$ negative-ion ground state [27]. The center-of-mass photoelectron energies for detachment from the negative-ion ground state ranged from 0.531 to 1.323 eV for the laser wavelengths used during this experiment. Broad photoelectron energy scans failed to reveal the presence of the Si^- 2D or 2P metastable negative-ion states during the course of the experiment. In addition to the study

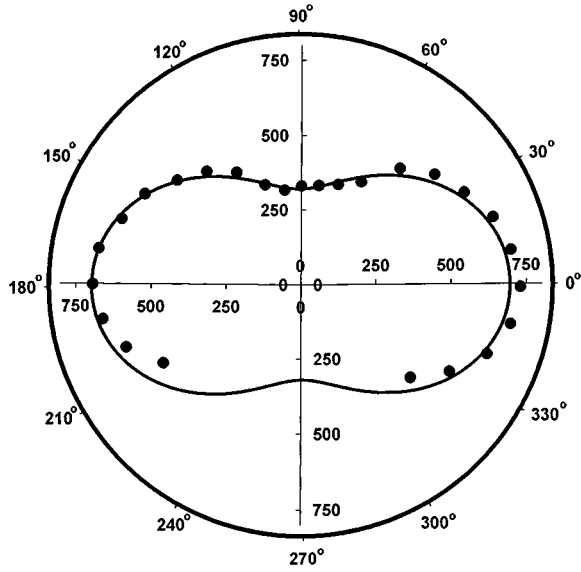


FIG. 4. Polar plot of a typical photoelectron yield-vs-linear polarization angle for Al^- at $\lambda = 514.5$ nm. The radial axis corresponds to the photoelectron yield and the angular axis to the laser polarization vector's angle with respect to the linear momentum vector of the collected photoelectrons. The experimental data points (solid circles) are given along with error bars associated with uncertainties in the photoelectron yields to one standard deviation. The solid line corresponds to a weighted nonlinear least-squares fit to the data producing an asymmetry parameter $\beta = 0.563 \pm 0.040$.

of $^{28}\text{Si}^-$, the asymmetry parameters for $^{29}\text{Si}^-$ and $^{30}\text{Si}^-$ were measured at a photon wavelength of 488.0 nm in order to test for possible isotopic effects in the angular distribution measurements. Isotopic substitution made little difference in the measured asymmetry parameter values. Plotted in Fig. 5 is a polar plot of a typical photoelectron yield as a function of polarization angle with respect to the electron collection direction for $\lambda = 514.5$ nm, along with a nonlinear least-squares fit of these data. The experimentally determined values of the asymmetry parameter for Si^- at all measured wavelengths are given in Table III, along with their respective experimental uncertainties.

D. Angular distributions of P^-

Angular distributions of photoelectrons liberated from P^- were measured at discrete visible photon energies ranging

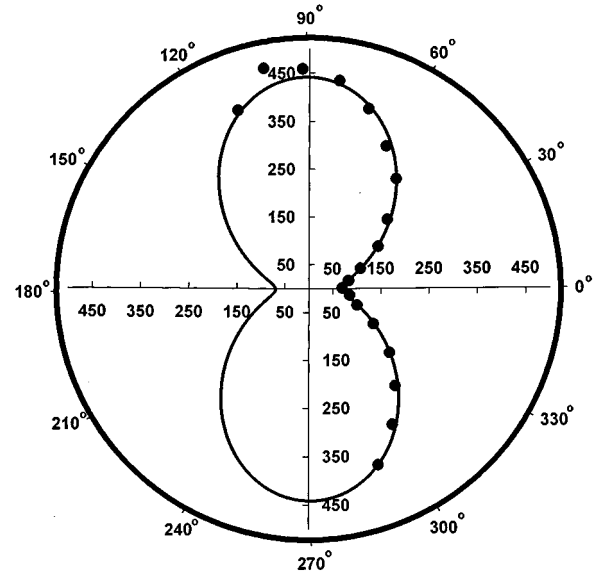


FIG. 5. Polar plot of a typical photoelectron yield-vs-linear polarization angle for the single-photon detachment of Si^- at $\lambda = 514.5$ nm. The radial axis corresponds to the photoelectron yield and the angular axis to the laser polarization vector's angle with respect to the momentum vector of the collected photoelectrons. The experimental data points (solid circles) are given along with error bars associated with uncertainties in the photoelectron yields to one standard deviation. The solid line represents a weighted nonlinear least-squares fit to the experimental data and produces an asymmetry parameter of $\beta = -0.782 \pm 0.008$.

from 1.92 to 2.71 eV in order to study the spectral variation of the asymmetry parameter. P^- negative-ion beams were produced with a sputter probe pressed from a 99% metal basis Mn_3P_2 powder. P^- -ion-beam currents produced were typically 100 nA, which produced signal-to-noise ratios of approximately 50:1. P^- has no known metastable states nor does it have more than one stable isotope to allow for labeling.

The photodetachment process for P^- can be described by $h\nu + \text{P}^-([\text{Ne}]3s^23p^4\ ^3P) \rightarrow \text{P}([\text{Ne}]3s^23p^3\ ^4S) + e^-(k_s, d)$. The electron affinity of P is defined as the difference between the total binding energy of the $^4S_{3/2}$ neutral atom ground state and the 3P_2 negative-ion ground state. Previous measurements have determined this value to be 0.7465 eV [28–30]. Hence, the center-of-mass photoelectron energies for this species ranged from 1.169 to 1.961 eV. A polar plot of

TABLE II. Asymmetry parameters for the single-photon detachment of Al^- at photoelectron energies ranging from 1.475 to 2.267 eV. Experimental results of the asymmetry parameter (β_{expt}) are tabulated along with the experimental error bars to one standard deviation of the mean. Also shown are the length and velocity form results of the recent calculation (β_{calc}) of Liu and Starace [1].

Photon wavelength λ (nm)	Photoelectron energy (eV)	Asymmetry parameter β_{expt}	Asymmetry parameter β_{calc} (length form)	Asymmetry parameter β_{calc} (velocity form)
647.1	1.475	0.30 ± 0.05	0.3783	0.6631
514.5	1.969	0.583 ± 0.024	0.6745	0.8548
488.0	2.100	0.644 ± 0.024	0.7347	0.8929
476.0	2.164	0.66 ± 0.06	0.7620	0.9103
457.9	2.267	0.730 ± 0.025	0.8036	0.9368

TABLE III. Asymmetry parameters for the single-photon detachment of Si^- at photoelectron energies ranging from 0.531 to 1.323 eV. Experimentally measured values of the asymmetry parameter (β_{expt}) are given along with experimental error bars to one standard deviation of the mean.

Photon wavelength λ (nm)	Photoelectron energy (eV)	Asymmetry parameter β_{expt}
647.1	0.531	-0.866 ± 0.024
514.5	1.025	-0.75 ± 0.04
488.0	1.156	-0.625 ± 0.008
476.0	1.220	-0.552 ± 0.020
457.9	1.323	-0.478 ± 0.011

the photoelectron yield as a function of polarization angle is given in Fig. 6 for P^- at a photon wavelength of 514.5 nm. Tabulated in Table IV are the experimental results of the asymmetry parameter for P^- along with their experimental uncertainties.

IV. DATA ANALYSIS

Within the framework of the independent-electron approximation, the bound valence electrons of all species contained in the present study occupy p orbitals. Therefore, the photodetached electron is represented by outgoing s and d partial waves. Near the photodetachment threshold, the s partial waves should dominate the behavior of the emission

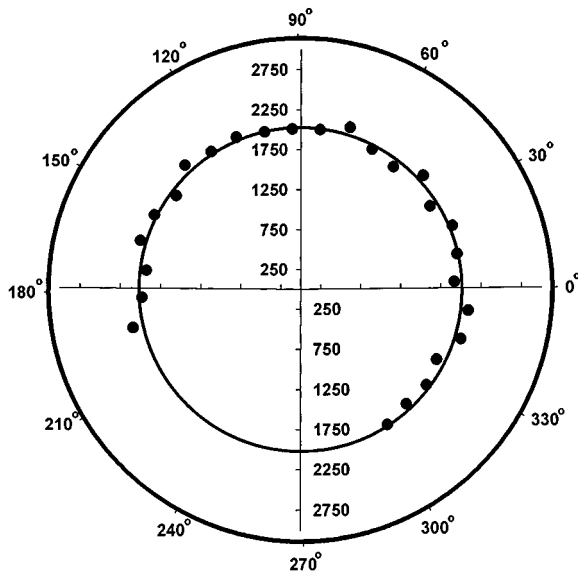


FIG. 6. Polar plot of a typical photoelectron yield-vs-polarization angle for the photodetachment of P^- at $\lambda = 514.5$ nm. The radial axis corresponds to the photoelectron yield and the angular axis to the laser polarization vector's angle with respect to the momentum vector of the collected photoelectrons. The experimental data points (solid circles) are given along with error bars associated with uncertainties in the photoelectron yields to one standard deviation. The solid line represents a weighted nonlinear least-squares fit to the experimental data and produces an asymmetry parameter of $\beta = -0.002 \pm 0.014$.

TABLE IV. Asymmetry parameters for the single-photon detachment of P^- at photoelectron energies ranging from 1.170 to 1.962 eV. The experimental determined values of the asymmetry parameter (β_{expt}) are tabulated along with experimental error bars representing one standard deviation of the mean.

Photon wavelength λ (nm)	Photoelectron energy (eV)	Asymmetry parameter β_{expt}
647.1	1.170	-0.247 ± 0.018
514.5	1.664	-0.013 ± 0.024
488.0	1.795	0.096 ± 0.021
476.0	1.859	0.110 ± 0.029
457.9	1.962	0.224 ± 0.015

pattern due to the suppression of d partial waves by the centrifugal barrier as described by the Wigner threshold law [31]. In contrast, for all measurements contained herein, the photoelectron energies are far from threshold, and so both s and p partial waves are likely to be present. The interference between these two competing partial wave channels is reflected in the pronounced spectral variation for each ion species studied at visible wavelengths. For the photodetachment of Al^- , the interaction of the liberated s and d partial wave electrons with the 2P neutral core allow for one parity-favored ($j_t=1$) and one parity-unfavored ($j_t=2$) angular-momentum transfer. Therefore, the asymmetry parameters and cross sections for both the parity-favored and -unfavored cases can be expressed as

$$\beta_{\text{fav}}(1) = \frac{|S_d(1)|^2 - \sqrt{2}[S_d(1)S_s^*(1) + S_d^*(1)S_s(1)]}{|S_d(1)|^2 + |S_s(1)|^2}, \quad (5)$$

$$\sigma_{\text{fav}}(1) = [|S_d(1)|^2 + |S_s(1)|^2], \quad (6)$$

$$\beta_{\text{unf}}(2) = -1, \quad (7)$$

$$\sigma_{\text{unf}}(2) = \frac{2}{3} |S_d(2)|^2, \quad (8)$$

and the effective value of the asymmetry parameter is given by Eq. (3). A similar analysis reveals that for both Si^- and P^- there is only one allowed value of angular-momentum transfer ($j_t=1$), and the effective asymmetry parameters and cross sections reduce to the forms of Eqs. (5) and (6) above. The overall form of the effective value of the asymmetry parameter for Al^- is identical in form to that obtained for B^- by Liu *et al.* [19]. However, the general shapes of the spectral variation seen between Al^- and B^- are qualitatively different, as can be seen in Fig. 7. These differences may be due to differences in the relative strengths of final-state interactions or to differences in the initial negative-ion states. Shown in Fig. 8 are the asymmetry parameters for Al^- , Si^- , and P^- plotted as a function of photoelectron energy. Although each of the species under investigation has been measured at different energies above the photodetachment threshold, the general shape of the spectral variation plots for each species is markedly different when taking into account the constraint $\beta=0$ near the photodetachment threshold. This pronounced difference may be due to different relative

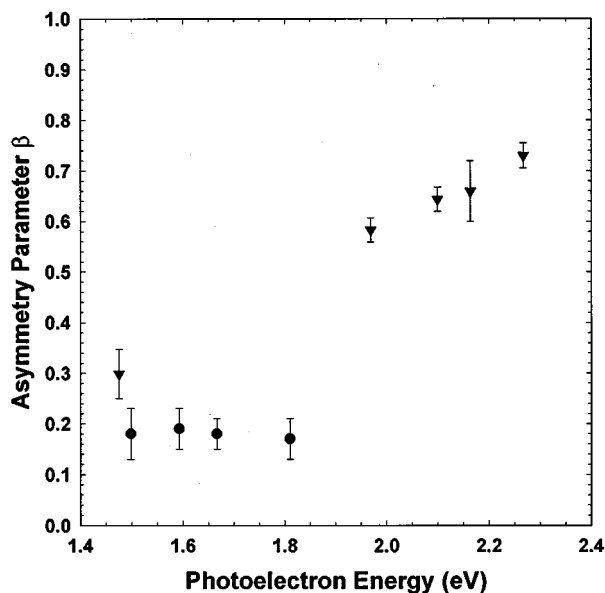


FIG. 7. Comparison of the spectral variation of the asymmetry parameter for B^- and Al^- . The experimental values for B^- (solid circles) [19] and for Al^- (inverted triangles) are given along with experimental error bars to one standard deviation. Although the form of the effective asymmetry parameter is identical for both single-photon detachment processes under the formalism of Fano and Dill [12], the spectral variation observed is markedly different.

strengths of the final-state interactions between the liberated electrons and their respective neutral cores or to differences in the initial negative-ion states. Recently, theoretical values of the asymmetry parameter were calculated [1] for the photodetachment of Al^- , using the eigenchannel R -matrix method [32,33]. These calculations are in good agreement with the present experimental measurements at visible photon energies. As can be seen from Table II, experimental and theoretical (length form) values of the asymmetry parameters for Al^- agree to within 20% in magnitude and there is very good agreement in the general shape of the spectral variation at measured photon energies.

V. CONCLUSIONS

Experimental measurements of the spectral variation of the asymmetry parameters have been made for the single-photon detachment of Al^- , Si^- , and P^- at discrete visible laser wavelengths. These measurements represent a systematic study of photoelectron angular distributions for complex negative ions with similar electronic structure spanning the visible photon energy regime. Experimental and theoretical values of the asymmetry parameter have been found to be in good agreement for Al^- at visible photon wavelengths [1]. A comparison has also been given between the measured values of the asymmetry parameters for Al^- and B^- [19]. Although the effective value of the asymmetry parameter for both species is identical within the formalism of angular-momentum transfer theory, the observed shape of the spectral variation is noticeably different. Within the confines of

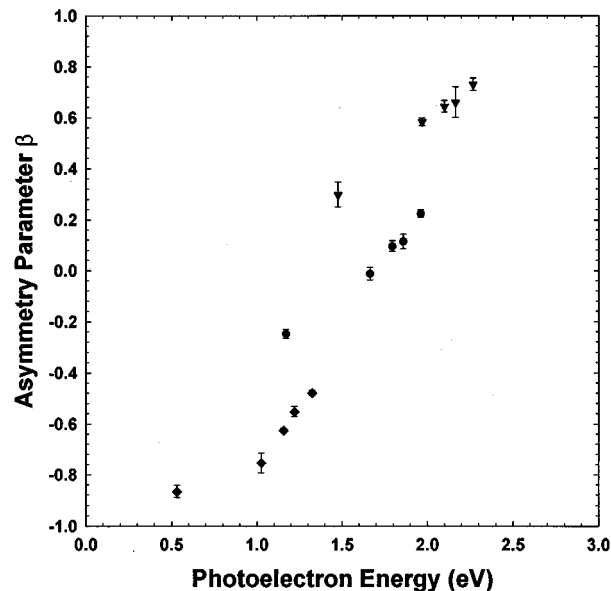


FIG. 8. Plot of the asymmetry parameter as a function of photoelectron energy for the photodetachment processes $Al^-(^3P) + h\nu \rightarrow Al(^2P) + e^-$ (inverted triangles), $Si^-(^4S) + h\nu \rightarrow Si(^3P) + e^-$ (diamonds), and $P^-(^3P) + h\nu \rightarrow P(^4S) + e^-$ (circles) along with the experimental error bars to one standard deviation. The energy dependence of the asymmetry parameter is clearly demonstrated for all three ionic species throughout the visible photon wavelength range measured.

the independent-particle approximation, one might expect the spectral variation of the asymmetry parameters to be very similar in nature for the negative ions in this study, since all photoelectrons originated from $3p$ orbitals. The markedly different behavior observed for each species defies any simple explanation. A complete theoretical calculation of photodetachment would need to include highly detailed information of the initial bound state as well as the phase-dependent description of the outgoing electrons in the presence of the residual field of the atomic core. It is hoped that these measurements will stimulate further theoretical investigations of photoelectron angular distributions following photodetachment. Theoretical investigations are needed to clarify the relative contributions of the various physical mechanisms governing the spectral variation in the observed photoelectron angular distributions.

ACKNOWLEDGMENTS

These experiments would not have been possible without the devoted technical assistance of UNR's departmental machinists Wade Cline, Dennis Meredith, and Walt Weaver and electronics technician William Brinsmead. Support from the NSF is gratefully acknowledged under Cooperative Agreement No. OSR 93-53227. T.J.K. gratefully acknowledges support from the Division of Chemical Sciences, Office of Basic Energy Science, Office of Energy Research, U.S. Department of Energy.

- [1] C. N. Liu and A. F. Starace, *Bull. Am. Phys. Soc.* **42**, 1026 (1997).
- [2] R. Wildt, *Astrophys. J.* **89**, 295 (1939).
- [3] H. S. W. Massey, *Negative Ions*, 3rd ed. (Cambridge University Press, London, 1976); B. M. Smirnov, *Negative Ions* (McGraw-Hill, New York, 1982).
- [4] P. G. Burke, *Atomic Processes and Applications*, edited by P. G. Burke and B. L. Moiseiwitsch (North-Holland, Amsterdam, 1976) pp. 242–290.
- [5] C. Blondel, C. Delsart, and F. Dulieu, *Phys. Rev. Lett.* **77**, 3755 (1996).
- [6] S. T. Manson and A. F. Starace, *Rev. Mod. Phys.* **54**, 389 (1982).
- [7] C. N. Yang, *Phys. Rev.* **74**, 764 (1948).
- [8] J. Cooper and R. N. Zare, in *Lectures in Theoretical Physics: Atomic Collision Processes*, edited by S. Geltman, K. T. Mahanthappa, and W. E. Britten (Gordon and Breach, New York, 1969), Vol. XI-C, p. 317.
- [9] J. Cooper and R. N. Zare, *J. Chem. Phys.* **48**, 942 (1968).
- [10] Dan Dill, *Phys. Rev. A* **7**, 1976 (1973).
- [11] Dan Dill, A. F. Starace, and Steven T. Manson, *Phys. Rev. A* **11**, 1596 (1975).
- [12] U. Fano and Dan Dill, *Phys. Rev. A* **6**, 185 (1972).
- [13] L. M. Branscomb and S. J. Smith, *Phys. Rev. Lett.* **98**, 1127 (1955).
- [14] L. M. Branscomb and S. J. Smith, *Phys. Rev.* **98**, 1028 (1955).
- [15] J. L. Hall and M. W. Siegel, *J. Chem. Phys.* **48**, 943 (1968).
- [16] H. Hotop and W. C. Lineberger, *J. Phys. Chem. Ref. Data* **14**, 731 (1985).
- [17] D. Hanstorp, C. Bengtsson, and D. J. Larson, *Phys. Rev. A* **40**, 670 (1989).
- [18] J. S. Thompson, D. J. Pegg, R. N. Compton, and G. D. Alton, *J. Phys. B Lett.* **23**, L15 (1990).
- [19] Y. Liu, D. J. Pegg, J. S. Thompson, J. Dellwo, and G. D. Alton, *J. Phys. B Lett.* **24**, L1 (1991).
- [20] Kingston Scientific Inc., Kingston, TN 37763.
- [21] D. Calabrese, A. M. Covington, and J. S. Thompson, *J. Chem. Phys. Lett.* **105**, 2937 (1996).
- [22] D. Calabrese, A. M. Covington, and J. S. Thompson, *Nucl. Instrum. Methods Phys. Res. A* **379**, 192 (1996).
- [23] N. Stolterfoht, *Phys. Rep.* **146**, 317 (1987).
- [24] D. Feldmann, *Chem. Phys. Lett.* **47**, 338 (1977).
- [25] D. Calabrese *et al.*, *J. Phys. B* (to be published).
- [26] D. Calabrese, A. M. Covington, J. S. Thompson, R. W. Marawar, and J. W. Farley, *Phys. Rev. A* **54**, 2797 (1996).
- [27] A. Kasdan, E. Herbst, and W. C. Lineberger, *J. Chem. Phys.* **62**, 541 (1975).
- [28] V. Radojevic, H. P. Kelly, and W. R. Johnson, *Phys. Rev. A* **35**, 2117 (1981).
- [29] D. Feldmann, *Z. Phys. A* **277**, 19 (1976).
- [30] J. Slater and W. C. Lineberger, *Phys. Rev. A* **15**, 2277 (1977).
- [31] E. P. Wigner, *Phys. Rev.* **73**, 1002 (1948).
- [32] U. Fano and C. M. Lee, *Phys. Rev. Lett.* **31**, 1573 (1973).
- [33] U. Fano and C. H. Greene, *Phys. Rev. A* **22**, 1760 (1980).